AALBORG UNIVERSITY

Estimating Atterberg limits of soils from reflectance spectroscopy and pedotransfer functions

Knadel, Maria; Ur Rehman, Hafeez; Pouladi, Nastaran; Wollesen de Jonge, Lis; Moldrup, Per; Arthur, Emmanuel

Estimating Atterberg limits of soils from reflectance spectroscopy and pedotransfer functions

Maria Knadel [a],[*], Hafeez Ur Rehman [b], Nastaran Pouladi [c], Lis Wollesen de Jonge [a], Per Moldrup [d], Emmanuel Arthur [a]

[a] *Dep. of Agroecology, Aarhus University, Blichers Alle 20, DK-8830 Tjele, Denmark*
[b] *Faculty of Science and Technology, Norwegian University of Life Science, Ås, Norway*
[c] *Dep. of Soil Science and Soil Protection, Food and Natural Resources, Czech University of Life Sciences, Prague, Czech Republic*
[d] *Dep. of Civil Engineering, Aalborg University, Thomas Manns Vej 23, Aalborg O 9200, Denmark*

ARTICLE INFO

ABSTRACT

Atterberg limits are broadly used for engineering and geology purposes as well as in agricultural and environmental applications. Laboratory methods used for their determination are, however, laborious, destructive and tool dependent. The aim of this study was to test the feasibility of using visible near-infrared spectroscopy (vis–NIRS) as a fast and accurate alternative to the conventional measurements of Atterberg limits (LL and PL) and the PI for 229 geographically diverse soil samples originating from 24 countries. Three types of calibration techniques including Partial Least Squares (PLS) regression, Artificial Neural Networks (ANN) and Support Vector Machines (SVM) were applied to the spectral data. The performance of the best vis–NIRS models was validated using 45 independent samples and compared with two existing and one newly developed pedotransfer functions (PTF). The application of SVM yielded marginally better predictive ability than PLS and ANN for all modelled properties. The SVM models estimated LL, PL, and PI with root mean squared error (RMSE) of 7%, 5% and 7%, respectively. The newly developed PTF gave slightly better estimations than the existing ones, with RMSE values of 8%, 6%, and 6%, respectively for LL, PL, and PI. Furthermore, in terms of the sample swelling class, the SVM model correctly classified 31 of the 45 samples, compared to 34 samples for the best PTF. The results indicate a great potential of vis–NIRS for reliable estimates of Atterberg limits for soil samples of large geographical and mineralogical diversity.

1. Introduction

Atterberg limits were introduced as measures of soil mechanical behaviour concerning the consistency limits of water content by Albert Atterberg (Atterberg, 1911). The limits include shrinkage limit (SL), plastic limit (PL), and liquid limit (LL) and define the transition of soil from solid to semisolid state, the point when the soil begins to act like plastic, and the transition from plastic to a liquid state, respectively. Additionally, the plasticity index (PI), calculated as a difference between LL and PL, is used as a measure of the plasticity of soil. Clayey soils tend to have a high PI whereas sandy soils are non-plastic (PI = 0). Atterberg

limits are broadly used in the Unified Soil Classification System for engineering and geology purposes as well as in agriculture (soil tillage, erosion) and environmental applications (Sivakumar et al., 2009; Keller and Dexter, 2012; Saikia et al., 2017; Obour et al., 2018). The limits can be employed in determining the soil shrink/swell potential, indicating the extent to which soils shrinks or swells when it dries or gets wet, respectively; useful for safe design, construction and maintenance of buildings on expansive soils.

The conventional laboratory methods for determining LL include the percussion method with the Casagrande cup ASTM (2017) and the drop-cone penetration method (BS, 2018). For PL, the most commonly used

method is the hand thread rolling (ASTM, 2017), further upgraded to the motorized rolling device (Bobrowski and Griekspoor, 1992). These methods share a common disadvantage of being laborious and costly especially when many samples need to be analysed. Moreover, they are all destructive and tool/laboratory setup dependent (Houlsby, 1982; Haigh, 2012; Spagnoli, 2012; Kayabali et al., 2016).

As alternatives to the above-mentioned laboratory methods, pedo-transfer functions (PTFs) for the determination of Atterberg limits from easily measurable or available soil properties were developed. These functions utilize soil properties such as texture, organic matter and pH (de Jonge et al., 1990; Seybold et al., 2008; Keller and Dexter, 2012; Gupta et al., 2016; Stanchi et al., 2017), or other properties like cation exchange capacity, specific surface area of the soil, and hygroscopic water content (Smith et al., 1985; Yukselen-Aksoy and Kaya, 2010; Arthur et al., 2021). As the magnitude of Atterberg limits is significantly affected by the clay mineral type (Schmitz et al., 2004), the majority of the PTFs are site-dependent and exhibit lower accuracy when used for samples that are mineralogically different from the samples used to develop the PTFs (Arthur et al., 2021). Consequently, it is of significant interest to consider alternative, rapid and reliable approaches to estimate the Atterberg limits, particularly for regional-scale studies. One potential approach is the application of visible near-infrared spectroscopy (vis–NIRS).

Visible near-infrared spectroscopy utilizes the characteristic absorption spectral features (in the wavelength range between 400 and 2500 nm) to identify the corresponding functional groups in a sample (Pasquini, 2003). The vis–NIRS method has been successfully applied to determine fundamental and functional soil properties such as organic matter (OM) and soil texture (Stenberg et al., 2010; Soriano-Disla et al., 2014; Hermansen et al., 2016; Hermansen et al., 2017), structural (Katuwal et al., 2018a; Katuwal et al., 2018b), surface (Knadel et al., 2018; Knadel et al., 2020) and hydraulic soil properties (Pittaki-Chrys-odonta et al., 2018; Pittaki-Chrysodonta et al., 2019; Santra et al., 2009). It is rapid, cheap and does not destroy the sample, requiring only little to no sample processing or chemicals. Soil properties such as clay and OM content and quality and water retention dictate soil mechanical behaviour and consequently the Atterberg limits (de Jonge et al., 1990; Keller and Dexter, 2012; Sridharan, 2014; Stanchi et al., 2017). These controlling properties (clay content, mineralogy, OM and water retention) have been successfully predicted using vis–NIRS (Rossel et al., 2009; Babaeian et al., 2015; Fang et al., 2018; Pittaki-Chrysodonta et al., 2019) thus, successful vis–NIRS estimations for the Atterberg limits can be expected. However, in comparison to the vast literature available on the vis–NIRS application to the determination of basic soil properties such as OM or texture, so far, only a few studies have investigated the possibility

for estimating Atterberg limits from vis–NIRS (Table 1). These studies were based on local data sets, including one to three sites and were each conducted on soil samples from one country. For example, the study by Waruru et al. (2014) utilized the highest number of samples (N = 256), however, the soils originated from only two sites in Kenya. Thus, there is difficulty in generalising the presented results. For the majority of studies, partial least squares (PLS) regression was employed to correlate soil spectra with Atterberg limits. Only two studies additionally tested the application of other techniques such as neural networks or support vector regression (Gupta et al., 2016; Mousavi et al., 2020) with only one comparing the results with newly developed pedotransfer functions (Gupta et al., 2016). Despite the different performance of vis–NIRS in the afore-mentioned studies (Table 1), there is a great potential of spectroscopy to estimate the Atterberg limits.

Considering the above-mentioned knowledge gaps, the objectives of this study were to (i) test and independently validate the capability of vis–NIRS for estimating Atterberg limits (PL and LL) and, PI for a dataset composed of different soil types and mineralogies representing diverse geographic origins, (ii) compare the performance of PLS regression to Artificial Neural Networks (ANN) and Support Vector Machines (SVM) techniques, and (iii) compare the vis–NIRS performance to existing pedotransfer functions (PTFs) from literature as well as one developed using the investigated dataset.

2. Materials and methods

2.1. Investigated soil samples

A total of 229 soil samples (topsoil and subsoil) was investigated. The samples were from 24 countries distributed across four continents: Africa (N = 47), Asia (N = 43) and Oceania (N = 12), Europe (N = 125) and South America (N = 2). The samples were selected to encompass a wide range of soil types (Vertisols, Chernozems, Luvisols, Oxisols, and Andisols), mineralogy (illite, montmorillonite, kaolinite and traces of chlorite and vermiculite) and serve as a basis for more universal models and generalizable results. Further details for the samples are provided in Table S1.

2.2. Data subdivision

To subdivide the dataset into calibration and validation sets, first, principal component analysis was conducted on the spectral data (Martens and Næs, 1989). Next, Kennard Stone algorithm (Kennard and Stone, 1969) was applied to the first three principal components and was set to select 80% (184 samples from 24 countries) samples to constitute

Table 1
Review table of published studies on the application of visible near-infrared spectroscopy to Atterberg limits (liquid limit; LL, plastic limit; PL, plasticity index; PI). Presented statistics are for the validation results.

Sample origin	Sample number calibration/validation	Property	Property range (%)	RMSEP (%)	SRMSE	R^2	Reference
Iran, Mount Alborz	45/15	LL	40–77	2	0.05	0.94	Mousavi et al. (2020)
		PL	25–31	3	0.50	0.55	
		PI	12–46	3	0.09	0.75	
Turkey, Ankara	62/21	LL	43–78	5	0.15	0.71	Rehman et al. (2019)
		PL	24–37	3	0.23	0.48	
India, West Bengal & N Odisha	128/54	LL	12–79	8	0.12	0.63	Gupta et al. (2016)
		PL	9–27	3	0.17	0.62	
		PI	0–47	9	0.20	0.32	
Kenya, Lake Victoria Basin	136/120	LL	22–97	10	0.13	0.74	Waruru et al. (2014)
		PL	11–45	NA	NA	0.46	
		PI	8–66	8	0.14	0.73	
Ethiopia, Addis Ababa	NA	LL	NA	0.5	NA	0.87	Yitagesu et al. (2009)
		PL		0.6		0.71	
		PI		0.5		0.81	

Where: RMSEP is root mean square error of prediction, SRMSE is RMSE/Range, NA indicates no information provided.

the calibration set. The remaining 20% (45 samples from 15 countries) was used for the independent validation of the generated calibration models. The application of Kennard-Stone algorithm enables a selection of representative samples spanning the widest range of their Euclidean distance within the spectral space (Kennard and Stone, 1969).

2.3. Laboratory measurements

2.3.1. Soil sieving

The samples were first crushed mechanically and sieved to 2-mm for the particle size fraction analyses. A part of the 2-mm sieved sample was crushed with a mortar and pestle to make them finer before subsequent sieving. The crushed samples were then sieved to 425 μm and used for the determination of the Atterberg limits and NIR scanning.

2.3.2. Soil texture and organic carbon

The clay, silt and sand contents were determined on the 2-mm sieved samples by a combination of wet sieving and pipette or hydrometer methods (Gee and Or, 2002). Before the analysis, organic matter and carbonates were removed for both groups. Soil organic carbon (SOC) was measured on ball-milled samples by oxidizing the carbon at 950 °C with an elemental analyzer coupled to a thermal conductivity detector (Thermo Fisher Scientific, Waltham, MA).

2.3.3. Atterberg limits analysis

The 425 μm-sieved sample was used to determine the Atterberg limits. In brief, LL was determined in triplicate with drop-cone penetrometer method as the water content at which a standard cone penetrated the soil to a depth of 20 mm in 5 s (BS, 2018). To determine PL, 30 g of samples was mixed with water until the sample became plastic. The sample was rolled into two short threads of 5–10 mm thickness. The threads were placed on the device and rolled to 3 mm diameter and the gravimetric water content at the breaking point of the thread was considered the PL. For both LL and PL, the gravimetric water content of the samples was determined by oven drying at 105 °C for at least 48 h. Detailed description of the Atterberg limits measurements is provided by Arthur et al. (2021).

The PI was calculated as a difference between LL and PL.

2.3.4. Vis–NIRS measurements

Spectral measurements were performed in a controlled laboratory. Both humidity and temperature were monitored with average values of 23 °C and 48%, respectively. Air-dried samples (425 μm-sieved) were scanned using a vis–NIRS spectrophotometer. About 50 g of each soil was placed in a sample holder equipped with a quartz window. Each prepared sample was scanned in seven areas of the sample holder to account for sample variability. These readings (absorbance values; Abs = [log (1/R)], where R is reflectance) were averaged into one spectrum and used in further analysis.

3. Modeling

3.1. Vis–NIRS modelling

Spectral models were developed using Matlab PLS Toolbox 8.7 (Eigenvector Research). Before modelling, different types of pre-processing methods, including 1st and 2nd derivative (Savitzky-Golay) and scatter corrections (multiplicative scatter correction and standard normal variate) were applied (Savitzky and Golay, 1964; Martens and Næs, 1989). However, only the results for the best preprocessing will be discussed further. Calibration models using PLS regression, ANN and SVM (segmented cross-validation; 20 randomly selected segments) were developed. The three methods are described in details elsewhere (Knadel et al., 2020) thus, only brief descriptions are given here. Among the linear regression techniques, PLS regression is most often applied to estimate soil properties from spectral data. It finds the latent variables in

spectral data which best estimate the soil property of interest by compressing and regressing the data. In this study, PLS regression with NIPALS algorithm was used (Martens and Næs, 1989; Wold et al., 2001). An ANN belongs to non-linear methods within machine-learning algorithms, which are to imitate the processes in human brain. The artificial neurons represent interconnected nodes within three layers, namely: vis–NIR spectra, the property to be predicted and a hidden layer between the two (Goldshleger et al., 2012). A feedforward ANN with a backpropagation neural network and PLS regression compressed spectra with two nodes in the first layer of the PC scores was performed (Rumelhart et al., 1986).

Support vector machines also represent a nonlinear method based on the kernel learning technique (here, Gaussian radial function was used) (Suykens and Vandewalle, 1999).

Two parameters were adjusted ε (used values: 1.0, 0.1, 0.01) and C (11 values from 10^{-3} to 100) representing the upper tolerance on prediction errors, and the trade-off between the model complexity and the degree to which deviations larger than ε are tolerated (Hastie et al., 2009).

Calibration models were evaluated using the root mean squared error of cross-validation (RMSECV), the root mean squared error of prediction (RMSEP), and the square of the Pearson correlation coefficient; R^2. The RMSECV and RMSEP are expressed in the same unit as the response variable *y* (here Atterberg limits or PI) and are calculated as follows:

$$RMSE = \sqrt{\frac{\sum\limits_{i=1}^{n}\left(y_p - y_m\right)^2}{n}} \tag{1}$$

where y_p is the average of the predicted values, y_m is the measured response values, and *n* is the number of samples.

Additionally, to enable the comparison of the results across the Atterberg limits and PI, the standardized RMSE was calculated as SRMSE = RMSE/Range (Arthur, 2017).

3.2. Pedotransfer functions

To compare the performance of the vis–NIRS to estimate the Atterberg limits and PI to PTFs, we selected two studies (de Jonge et al., 1990; Keller and Dexter, 2012) that utilized different combinations of clay, sand and organic carbon (OC), or OM contents.

The PTFs (Eqs. (2) to (4)) by de Jong et al. (1990) were developed from 279 samples obtained from Saskatchewan, Canada. The equations are presented below:

$$LL = 13.75 + 0.637 \times clay + 2.937 \times OC \tag{2}$$

$$PL = 10.95 + 0.239 \times clay + 1.156 \times OC \tag{3}$$

$$PI = 3.11 + 0.394 \times clay + 1.726 \times OC \tag{4}$$

The PTFs (Eqs. (5) to (7)) by Keller and Dexter (2012) was based on 89 samples from nine countries:

$$LL = 6.65 + 0.626 \times clay + 0.007 \times clay^2 + 7.40 \times OM - 0.128 \times clay \times OM \tag{5}$$

$$PL = 14.22 + 0.005 \times clay^2 + 3.63 \times OM - 0.048 \times clay \times OM \tag{6}$$

$$PI = -0.056 + 0.432 \times clay + 0.005 \times clay^2 - 0.167 \times sand + 2.79 \times OM - clay \times OM \tag{7}$$

Additionally, PTF functions using the calibration data set and basic soil properties were developed for comparison:

$$LL = 10.64 + 0.86 \times clay + 0.16 \times silt + 3.25 \times OC$$

$$adjusted\ R^2 = 0.68; SEE = 10.9 \tag{8}$$

$$PL = 8.70 + 0.29 \times clay + 0.07 \times silt + 2.90 \times OC$$

$$adjusted\ R^2 = 0.30; SEE = 10.1 \tag{9}$$

$$PI = 1.66 + 0.56 \times clay + 0.09 \times silt + 0.34 \times OC$$

$$adjusted\ R^2 = 0.57; SEE = 8.53 \tag{10}$$

4. Results and discussion

4.1. Description of dataset

The investigated samples represented soils varying in both texture and OC content covering from clayey (up to 89% clay) to sandy (up to 85% sand) and from mineral (average OC of 1.44%) to organic (average OC of 6.79%), thus representing all soil types in the USDA classification, except sand and silt (Fig. 1a and Table 2).

The soil types included Andisols, Luvisols, Oxisols, Vertisols, Chernozems etc, reflected by the different dominant clay minerals present (e. g., montmorillonite, kaolinite, illite, smectite – Table S1). This high variability of the data set was reflected in the wide range in the Atterberg limits and PI. Liquid limit covered a range from 20 to 106%, PL from 12 to 74% and PI from 3 to 59% (Table 2). Likewise, the samples comprised a wide range in swelling potential (according to the Casagrande plasticity chart) covering all five classes (low, medium, high, very high and few examples of extremely high) (Fig. 1 b).

The selection of calibration samples using the Kennard-Stone algorithm assured a full coverage of the ranges of the investigated soil properties including both Atterberg limits and PI (Fig. 1 and Table 2).

Atterberg limits were individually correlated with clay, silt, sand and OC contents (Fig. 2 and Table 3). As expected they were correlated more strongly with clay. Clay content and clay mineralogy are among the most important factors controlling Atterberg limits. Thus, among the three basic properties, the liquid limit was highest and significantly correlated with clay content ($r = 0.77$) (Fig. 2 a). The plastic limit was also significantly correlated with clay content ($r = 0.41$), yet to a lower degree than LL. In general, for samples with PL values above 40%, no clear trend in respect to correlations with other soil properties was observed. For example, samples exhibiting high PL values had both low sand (some of the Turkish samples) and high sand (New Zealand and Japan) contents (Fig. 2 g). Both the LL and PL were significantly correlated with OC, obtaining r values of 0.30 and 0.40, respectively.

Similar to LL, PI was strongly correlated with clay ($r = 0.76$) (Fig. 2 i), however, it was not significantly correlated with OC content (Fig. 2 l). Neither Atterberg limits, nor PI was significantly correlated with silt content for this data set (Fig. 2 b, f, and j). The results from this study are consistent with previous studies. A higher correlation between clay content and LL than with PL was found by for example Keller and Dexter (2012) and Stanchi et al. (2017). As suggested by Stanchi et al. (2017), PL is more controlled by the amount of organic C, whereas LL and PI are controlled by the clay fraction and the degree of aggregation resulting from interactions with soil OM. The authors explained this phenomenon by the interactions between clay and water during increasing water content. In the first stage of increasing water content (semisolid or plastic state, when all pores are filled with water) it is soil OM that retains additional water. Further, in the transition phase from plastic to the liquid state, it is the clay minerals that absorb water and play a more important role in LL behaviour (Stanchi et al., 2017).

4.2. Vis–NIRS characteristics of the soils

Visible near-infrared spectra of soils representing the five swelling potential classes (based on Casagrande's plasticity chart) are shown in Fig. 3. As discussed above, the Atterberg limits are correlated with clay content but more specifically with spectrally active clay minerals. Thus, there is a clear trend between absorbance and the swelling potential for the first four classes. In the NIR region, absorbance increases with swelling potential. In the regions typically assigned to absorptions related to OH bonds (near 1400, 1900 and 2200) (Clark et al., 1990; Ben-Dor and Banin, 1995) there is an increase in absorbance with the increase in the swelling potential class. The lowest absorption values for the samples with low swelling potential and vice versa can be also observed (Fig. 3). However, the spectra representing the soils with the extremely high swelling potential (marked in red in Fig. 3) behaved differently. Despite the very distinct absorptions related to OH bonds resulting from the extreme clay contents (above 80%), their total absorbance throughout the vis–NIR region was the lowest among all the classes and reflects their basic composition including very high clay content, mineralogy (dominated by montmorillonite) and very low OC content (mean OC of 0.11%). These soils are of a light grey colour and thus absorb comparatively less light than the remaining darker soils. In the visible part of the spectrum, similar trends to the NIR range can be observed. However, the spectrum of the soil with the high swelling potential shows higher absorbance values than that of a very high swelling class, due to the effects of high OC content in the first sample (3%) as opposed to the latter one (1.1%).
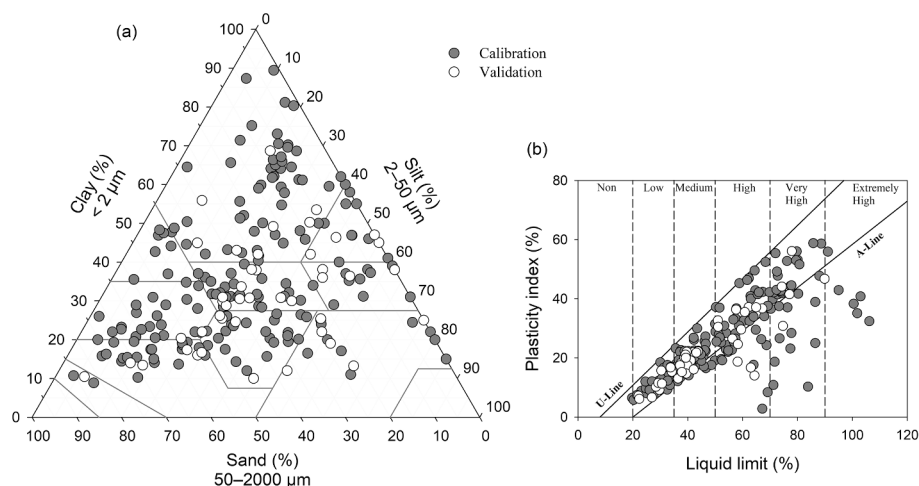

Fig. 1. a). Distribution of the investigated samples in the USDA soil textural triangle and b) Distribution of the investigated samples in the Casagrande plasticity chart (calibration set; $N = 184$, validation set, $N = 45$).

Table 2
General statistics for the liquid limit (LL), plastic limit (PL), plasticity index (PI), soil texture and organic carbon (OC) (unit for all – %) for the entire data set, calibration and validation sets.

Property	Mean	Max	Min	Range	SD	CV	Variance	Median
LL	51 (52, 47)	106 (106, 90)	20 (20, 22)	86 (86, 68)	19 (19, 17)	0.37 (0.37, 0.35)	349 (367, 274)	46 (47, 42)
PL	26 (26, 25)	74 (74, 50)	12 (12, 15)	62 (62, 36)	11 (12, 9)	0.44 (0.46, 0.35)	131 (145, 75)	23 (23, 21)
PI	25 (26, 23)	59 (59, 56)	3 (3, 6)	56 (56, 50)	13 (13, 11)	0.51 (0.51, 0.50)	164 (171, 132)	22 (22, 20)
Clay	36 (37, 32)	89 (89, 69)	9 (9, 10)	81 (81, 59)	17 (18, 14)	0.49 (0.49, 0.43)	299 (323, 189)	31 (32, 31)
Silt	31 (30, 36)	85 (85, 75)	2 (2, 6)	83 (83, 69)	17 (17, 15)	0.55 (0.58, 0.42)	291 (299, 230)	28 (26, 31)
Sand	33 (34, 32)	85 (85, 83)	0 (0, 0)	85 (85, 83)	22 (22, 20)	0.66 (0.66, 0.63)	479 (499, 402)	33 (33, 32)
OC	1.56 (1.63, 1.26)	8.23 (8.23, 4.64)	0 (0, 0)	8.23 (8.23, 4.64)	1.39 (1.43, 1.2)	0.90 (0.88, 0.95)	1.95 (2.05, 1.44)	1.37 (1.44, 0.81)

Note: the first value is for the entire data set ($N = 229$), the first value in the brackets is for the calibration dataset ($N = 184$), and the second value in the brackets is for the validation dataset ($N = 45$). SD, standard deviation, CV, coefficient of variation.
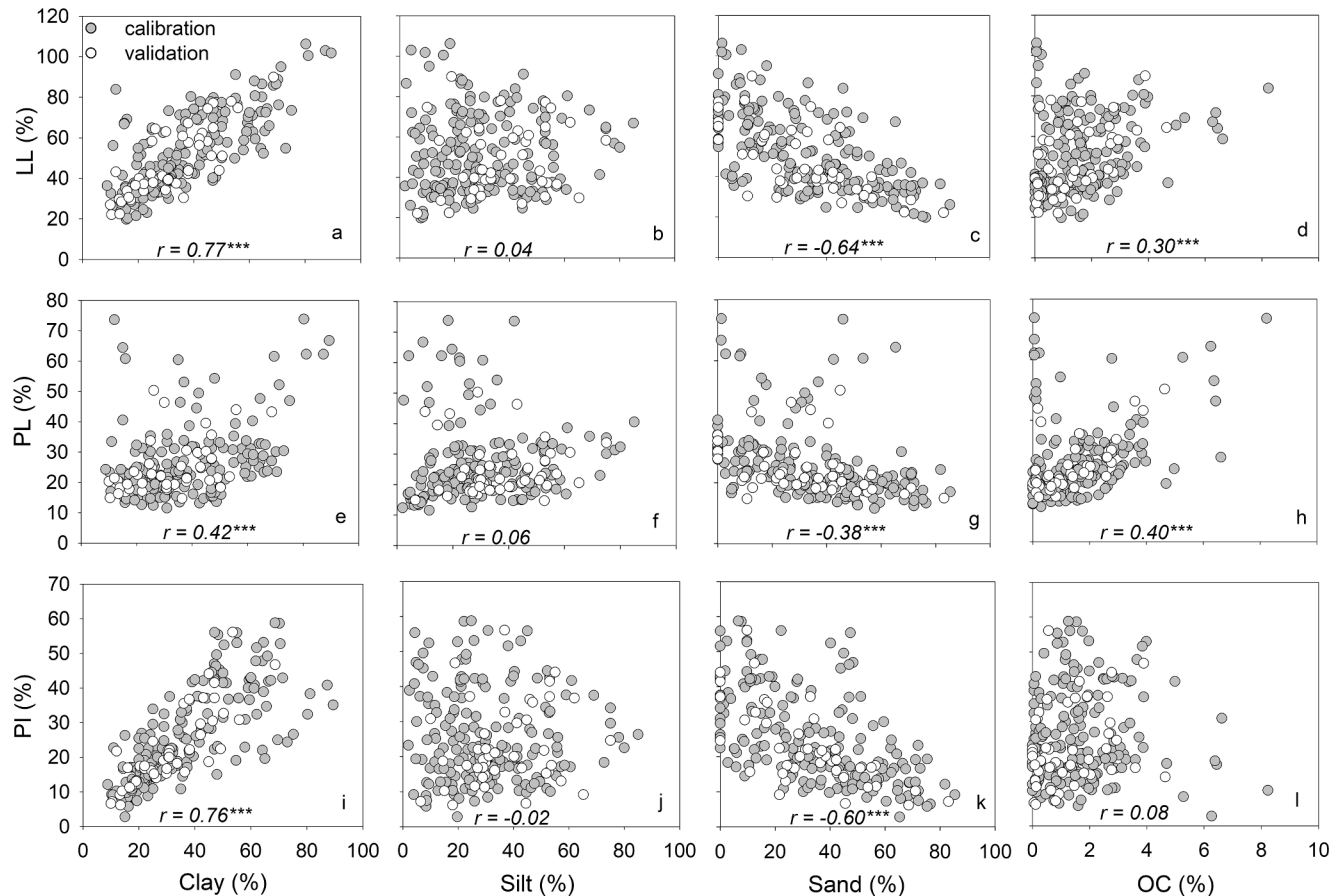

Fig. 2. Correlation between plastic limit; PL, liquid limit; LL and plasticity index; PI with clay, silt, sand and OC content for the entire data set. ***, **, and * denote statistical significance of the correlation coefficients at $P < 0.001$, 0.01 and 0.05, respectively.

4.3. Spectral calibration models

Calibration results for LL were similar for the three (PLS, ANN and SVM) tested techniques (Fig. 4 a, d and g). Both ANN and SVM generated the same errors (RMSECV of 10%) that were only slightly lower than the one generated by PLS regression (11%). PLS regression coefficients (not showed) for the LL model indicated the highest contribution of wavelengths are located at ~1900, ~2300, and ~1440 nm, all of which can be assigned to OH bonds (Post and Noble, 1993; Clark, 1999; Bishop et al., 1994), ~500 nm and in a range between 660 and 860 nm which are related to the presence of iron oxides (Scheinost, 1998; Hunt, 1977).

Likewise, small differences for PL estimations and between the techniques were observed. Here, PLS and ANN calibration models resulted in the same estimation error (7%) (Fig. 4 b and e) whereas, the RMSECV of the SVM model for PL was insignificantly lower (6%) (Fig. 4 h). The important wavelengths for PL used in the PLS regression model were very similar to those from the LL model and included bands near 1400, 1900 and 2300 nm. However, a slightly higher contribution of OH bonds around 1440 nm than in the LL model was found, and a negative regression coefficient around 500 nm.

As in the case of LL estimations, machine learning algorithms (SVM and ANN) delivered the lowest error for PI (7%) (Fig. 4 f and i) which was only slightly better than that for PLS regression (6%) (Fig. 4 c). In the visible part of the spectral range, the high regression coefficient observed around 560 nm originate from iron oxides (Scheinost, 1998). Whereas, in the NIR range a broad band 960–1250 nm (corresponding to iron oxides and possible OM; Scheinost, 1998) and bands near 1400, 1900 and 2300 nm (as in the case of LL and PL models) were present, and confirm an important role of clay content and mineralogy in the determination of the two Atterberg limits and PI.

Table 3
Performance of three pedotransfer functions; two from the literature (de Jonge et al. (1990) and Keller and Dexter, 2012) and one developed using the investigated data set (current PFT) and visible near-infrared spectroscopy estimations using support vector machine (vis–NIRS$_{SVM}$) for the liquid limit; LL, plastic limit; PL, and plasticity index; PI for the validation data set (N = 45).

Property	Estimation method	RMSEP	SRMSEP	R^2
LL (%)	de Jonge et al. (1990)	13	0.19	0.79
	Keller and Dexter (2012)	9	0.13	0.75
	Current PTF	8	0.12	0.79
	vis–NIRS$_{SVM}$	7	0.10	0.80
PL (%)	de Jonge et al. (1990)	8	0.22	0.36
	Keller and Dexter (2012)	6	0.17	0.57
	Current PTF	6	0.17	0.48
	vis–NIRS$_{SVM}$	5	0.14	0.64
PI (%)	de Jonge et al. (1990)	7	0.14	0.73
	Keller and Dexter (2012)	9	0.18	0.67
	Current PTF	6	0.12	0.73
	vis–NIRS$_{SVM}$	7	0.14	0.69

RMSEP, root mean square error of prediction, SRMSEP, standardized RMSEP.
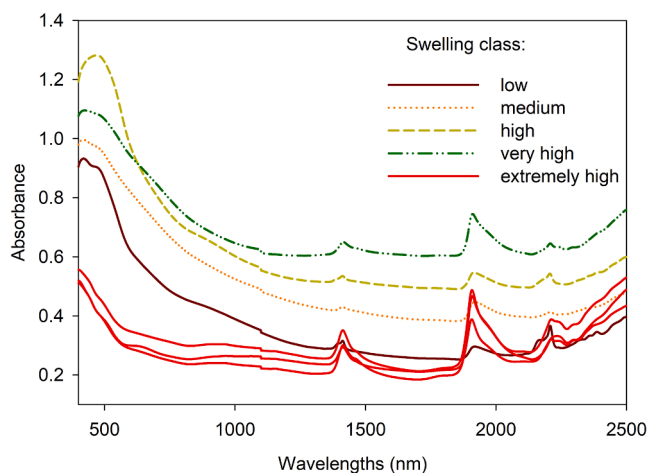

Fig. 3. Average visible near-infrared spectra per swelling class.

In general, the differences in model performance of the three modelling techniques and for each of the Atterberg limit were small and smallest for the error values and manifested mostly in the values of the coefficient of determination, which were consistently highest for the SVM technique. To test whether the estimations of Atterberg limits differ significantly among the modelling techniques, a one-way analysis of variance (ANOVA) on the residuals was additionally performed. The differences among the residual values from the three regression methods calculated for LL, PL and PI were not significant (P = 0.990, P = 0.366, and P = 0.913, respectively), indicating that using the commonly applied PLS regression produces similar results to that of more sophisticated algorithms such as SVM.

4.4. Validation results

The independent validation of the three regression techniques, using 45 samples, is presented in Fig. 5. For LL and PL, the SVM technique had the lowest prediction errors (RMSEP of 7 and 5%, respectively) and the highest R^2 values (>0.64) among the three techniques.

The application of ANN was nearly identical to that of PLS regression for LL and PL estimations (Fig. 5 a, d, b, e), generating the same prediction errors (9% and 6%, respectively).

The PI was estimated with the same prediction error (RMSEP of 7%) using ANN and SVM (Fig. 5 f and i), which was slightly lower than when using PLS (RMSEP = 8%) (Fig. 5 c). Moreover, the SVM model for PI had

the highest R^2 value (0.69). Additionally, the PI values estimated directly by SVM were compared to the PI calculated from the SVM-predicted LL and PL values. The slope of the equation (y = 0.9674x + 0.7283) and high correlation (r = 0.98) between the two PI estimations indicates stable results regardless of the approach.

A few of the samples were consistently under-predicted by the models. These samples represent special samples in terms of basic soil properties and mineralogy and as a consequence the Atterberg limits. They were identified and discussed previously in Fig. 2 g (some of the samples from New Zealand, had large amounts of amorphous minerals (e.g., volcanic glass) and had very high values for the Atterberg limits) and in Fig. 3 (the red spectra represent the extremely high swelling montmorillonite-rich samples from Turkey). Moreover, one of the Croatian samples with the lowest LL and PL tended to be significantly overestimated by all the models. However, no clear reasons for these overestimations were found. These samples were not removed from the modelling as they were not outliers per se but soil samples that have markedly different characteristics.

Despite some differences in models performance, the ANOVA test indicated that there is no statistically significant difference among the applied regression techniques to predict LL (P = 0.868), PL (P = 0.980) and PI (P = 0.970). However, to compare model performance among the three estimated properties the output of SVM modelling was chosen as it consistently generated the highest R^2 values.

To enable comparison of the three properties that have a different range in values, the SRMSE values were used. The LL estimations yielded the lowest SRMSE value of 0.10, compared to 0.14 for both PL and PI. These results can be explained by the correlations of Atterberg limits with spectrally active soil components as well as by the variability of Atterberg limits. For the validation dataset, LL is strongly correlated with clay content (r = 0.80) and OC content (r = 0.51). Both clay and OC in turn, are spectrally active in the visible and NIR range, leading to better estimation of LL. Conversely, PL was not as strongly correlated with clay (r = 0.45) as LL or PI, but was significantly correlated with OC (r = 0.68), whereas, PI was not correlated with OC at all (Table 3). Moreover, the accuracy of the models can be a result of data set variability, the higher the variability the lower accuracy (Brunet et al., 2007; Stenberg et al., 2010). When investigating the coefficient of variation (CV) for the three properties, LL had the lowest variability (37%) of them all (Table 2). This low variability, together with the significant correlation between LL with clay and OC could have led to better predictions for LL, compared to PL and PI.

Results from this study are comparable with the results published previously (Table 1). In the recent study by Mousavi et al. (2020) 60 samples from an experimental forest in Mount Alborz, Tehran were investigated. Atterberg limits were correlated with vis–NIR spectra using PLS regression, a PLS with back propagation neural networks as well as spectral indices. To validate models' performance a small set of 15 samples was used. Out of the three tested techniques, PLS BPNN generated the most accurate models for LL, PI (SRMSEP of 0.05 and 0.09, respectively) indicating a higher predictive ability than in the present study. However, they reported more than three times lower accuracy for the estimation of PL (SRMSEP = 0.5) than it was obtained here (SRMSEP = 0.14). Rehman et al. (2019) estimated Atterberg limits using vis–NIRS and compared two conventional methods for each Atterberg limit using a set of 83 Turkish samples. They obtained successful estimations of LL (SRMSEP = 0.15) and less robust PL models (SRMSEP = 0.22), both representing higher errors than in the present study. Several approaches to Atterberg limits' estimation using vis–NIRS and mid-infrared (MIR) regions and a set of 182 soil samples originating from India were reported by Gupta et al. (2016). The authors compared the performance of PLS, PLS with a feature selection, stepwise multiple regression (SMLR) and support vector regression (SVR). To test generated models 30% of the entire data set was used. The lower predictive ability for vis–NIRS than for MIR was obtained and the results for PLS and SVR were very similar generating nearly identical results, for both
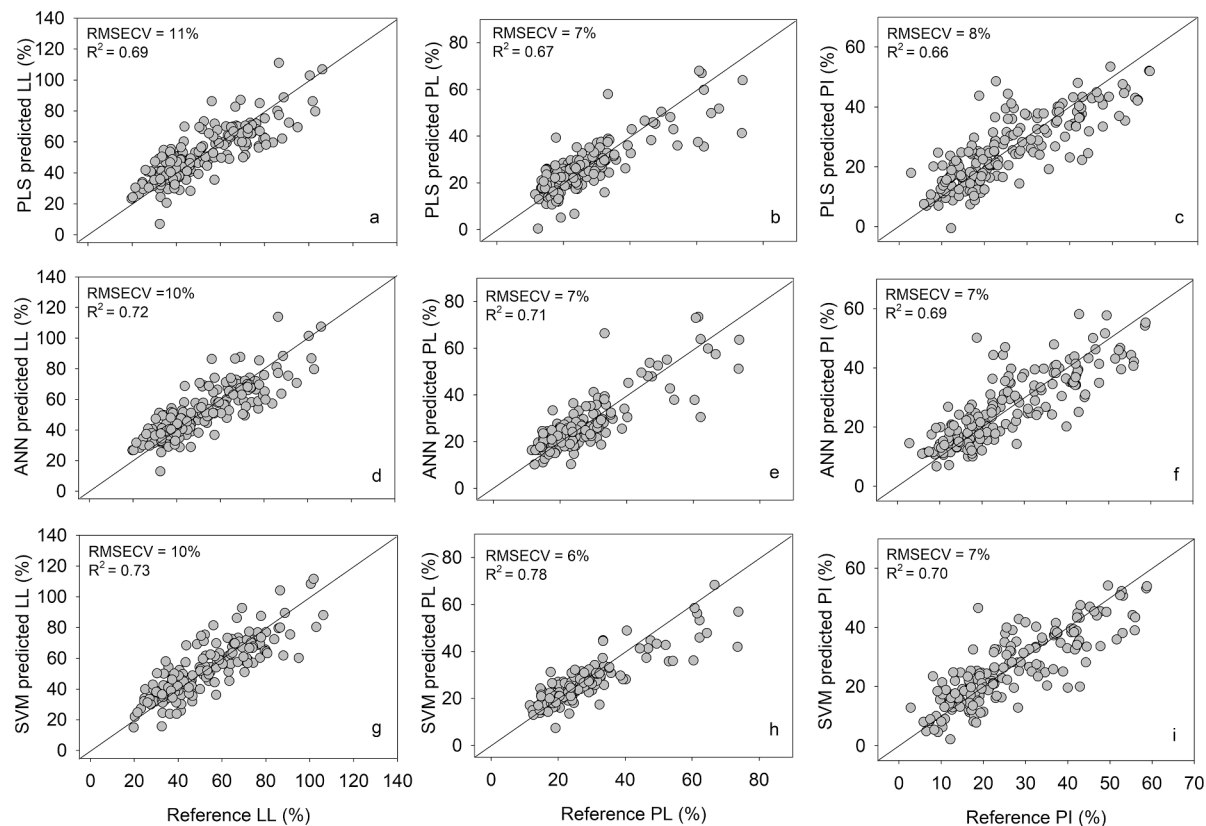
Fig. 4. Visible near-infrared spectroscopy calibration results ($N = 184$) for the Atterberg limits presented as predicted vs. measured for the liquid limit; LL (a, d, g), plastic limit; PL (b, e, h), and plasticity index; PI (c, f, I) generated using partial least squares (PLS), artificial neural networks (ANN), and support vector machine (SVM) regression techniques. RMSECV is the root mean square error of cross-validation.

errors and coefficient of determination, resulting in SRMSEP of 0.12, 0.17, and 0.20 for LL, PL and PI, respectively, thus less accurate than in this study. As the authors did not provide the ranges for the validation data set separately but for the entire data set only, we estimated the ranges from the provided predicted vs measured plots to calculate the SRMSEP values. The predictive ability for LL and PI models (SRMSEP of 0.13 and 0.14, respectively) generated for some Kenyan soils (Waruru et al., 2014) was lower for LL and the same for PI as generated by the SVM in this study. As no ranges for PL were given it was not possible to calculate the SRMSEP for the estimations on Kenyan soils, but the coefficient of determination for PL was much lower (0.44) than for LL (0.74) and PI (0.73), thus a less robust model than for the two properties is expected. A direct comparison, using SRMSEP, with the study by Yitagesu et al. (2009) is not possible as the authors did not provide information on the sample number or ranges of Atterberg limits and PI, and listed correlation coefficients only.

4.5. Comparison with pedotransfer functions

The prediction of LL, PL, and PI from two existing pedotransfer functions (PTFs) and a newly developed PTF based on the calibration dataset are presented in Table 3. The selected PTFs included clay, OC or OM and sand contents, whereas the new PTF included clay, silt and OC contents. These results were compared further with the vis–NIRS$_{SVM}$ results (Table 3).

Among the three PTFs, the newly developed one had the best results (RMSEP = 8%; R^2 = 0.79) for LL estimation. However, this result was similar to the one obtained by Keller and Dexter (2012) PTF (RMSEP = 9%). Likewise, Keller and Dexter (2012) PTF had a lower error for PL estimation (RMSEP = 6%) than the PTF of de Jonge et al. (1990) (8%) and the same error as the newly developed PTF.

Conversely, the de Jonge et al. (1990) PTF had a higher accuracy (RMSEP = 7%) than the Keller and Dexter (2012) PTF (RMSEP = 9%) and was similar to the newly developed PTF (RMSEP = 6%) for the estimation of PI.

Gupta et al. (2016) calculated also PTFs for the set of Indian samples and including available information on soil texture, pH and OC. They obtained SRMSEP of 0.11, 0.16, and 0.18 for LL, PL and PI, respectively (Table 1). Thus, a comparable accuracy for LL and PL and a lower accuracy for PI, than obtained by the PTFs used in this study (0.12, 0.17, 0.12, respectively) (Table 3).

The results of the best PTFs (newly developed functions) were comparable to these of the vis–NIRS$_{SVM}$ models. For the LL and PL estimations, the prediction errors were lowest when using spectroscopy (RMSEP of 7 and 5%, respectively). Whereas, the prediction error for PI was slightly lower when using the PTF to that generated by the vis–NIRS$_{SVM}$ model (RMSEP = 7%).

Additional t-tests of the residuals indicated no significant difference between vis–NIRS$_{SVM}$ and the PTFs for LL, PL as well as PI estimations (with reported P values of 0.508, 0.790, and 0.072, respectively).

Gupta et al. (2016) compared also the performance of pedotransfer functions to, among others, spectral models. The authors concluded that models based on spectral data were better for Atterberg limits than PTFs utilizing the information from the basic properties only. However, the differences were small and it was not tested whether they were significant.

4.6. Swelling potential classification

In the final analysis, the Casagrande plasticity chart was used to classify the swelling potential of the soils and the percentage of the samples classified into the correct swelling class using vis–NIRS$_{SVM}$ and
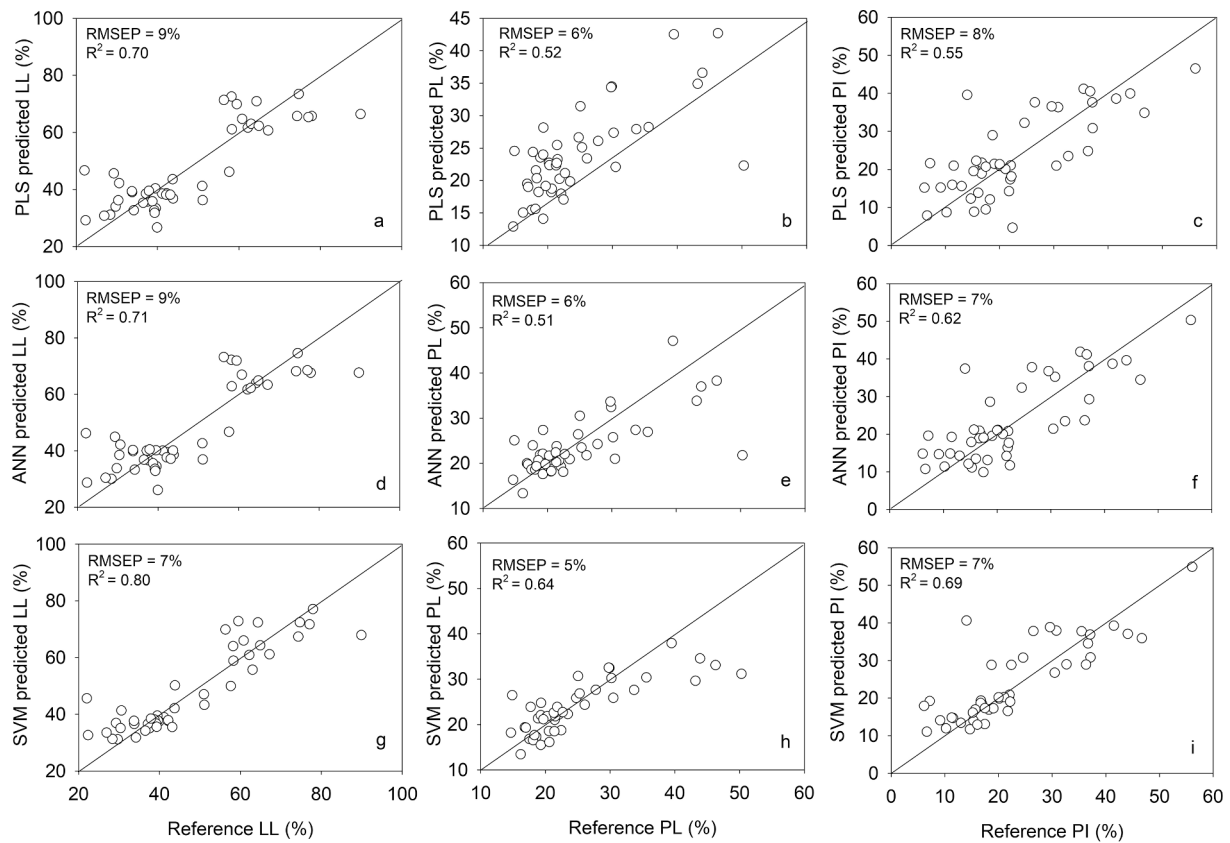
Fig. 5. Visible near-infrared spectroscopy independent validation ($N = 45$) for the Atterberg limits presented as predicted vs. measured for the liquid limit; LL (a, d, g), plastic limit; PL (b, e, h), and plasticity index; PI (c, f, I) generated using partial least squares (PLS), artificial neural networks (ANN), and support vector machine (SVM) regression techniques. RMSEP is the root mean square error of prediction.

newly developed PTF estimated LL was calculated and compared (Table 4). The values of the reference, vis–NIRS$_{SVM}$ and PTF predicted LL were plotted also in the Casagrande plasticity chart including the classification of swelling classes (Fig. 6).

The percentage of samples that were classified into the correct class for vis–NIRS$_{SVM}$ was the highest for the medium (88%) and high classes (67%) and decreased substantially for the low swelling potential class (55%).

The samples classified with the lowest accuracy were soils of some of the lowest and the highest LL values representing soils from Croatia, and Turkey, respectively (Fig. 6). Turkish soils were discussed previously as samples with very different colouration (Fig. 3). The classification of swelling potential according to the PTF estimates showed higher accuracy for the low class (64%), but lower for the medium and very low for the very high class (with only one sample out of five that was classified correctly). In turn, the PTF was able to correctly classify all samples within the high class (Table 4, Fig. 6).

In summary, 69 and 76% of the validation data set were correctly

Table 4

Percentage of the samples classified into the correct swelling class after estimation of liquid limit (LL) using the visible near-infrared spectroscopy and the pedotransfer function for the validation set ($N = 45$).

Swelling class based on LL	Percent vis–NIRS$_{SVM}$ correctly classified	Percent PTFs correctly classified
Low [11]	55	64
Medium [16]	88	81
High [12]	67	100
Very high [5]	60	20

Note: In the square brackets is the number of samples classified based on the reference method.
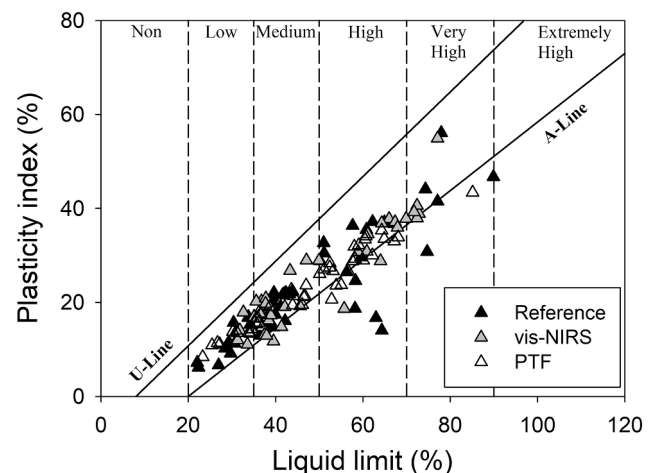

Fig. 6. Distribution of the reference samples (black triangles), the samples predicted by the visible near-infrared spectroscopy (grey triangles) and by the PTF (opened triangles) in the Casagrande plasticity chart.

classified by vis–NIRS$_{SVM}$ and the PTF, respectively. This corresponded to a small difference of three samples only (PTF correctly classified 34 whereas vis–NIRS$_{SVM}$ 31 samples) thus, very comparable results for the two approaches.

5. Conclusions

In this study, vis–NIRS and PTFs were applied for Atterberg limits and PI estimation for a set of soils representing large geographical and

clay mineralogical diversity. Three types of calibration techniques were compared for spectral modelling and included PLS regression, ANN and SVM. In general, the three regression techniques had statistically similar prediction accuracy. However, based on the R^2 and prediction errors, the SVM tended to have a better predictive ability for both Atterberg limits and PI. Additionally, it was found that PI directly estimated by vis–NIRS was similar to that computed from vis–NIRS estimated LL and PL.

Three pedotransfer functions including two available from the literature and one newly developed were further utilized and compared. The newly developed PTF outperformed the PTF available from the literature for LL and PI, and for PL, it had the same prediction error as the Keller and Dexter (2012) PTF.

When comparing the performance of vis–NIRS and the newly developed PTFs to predict LL, PL, and PI, as well as for the classification of the samples into swelling classes, there were no significant differences. Thus, taking into account the high variability of investigated soils, encompassing wide ranges of soil texture, clay mineralogy and OC content, the vis–NIRS models were as reliable as the best PTFs. Moreover, vis–NIRS can provide an alternative method to the estimation of several soil properties, which can be simultaneously derived from the same spectral measurement.

Declaration of Competing Interest

The authors declare that they have no known competing financial interests or personal relationships that could have appeared to influence the work reported in this paper.

Acknowledgements

Appendix A. Supplementary data

Supplementary data to this article can be found online at https://doi.org/10.1016/j.geoderma.2021.115300.

References

Arthur, E., 2017. Rapid estimation of cation exchange capacity from soil water content. Eur. J. Soil Sci. 68, 365–373.

Arthur, E., Rehman, H.U., Tuller, M., Pouladi, N., Norgaard, T., Moldrup, P., de Jonge, L. W., 2021. Estimating Atterberg limits of soils from hygroscopic water content. Geoderma 381.

ASTM D4318–17e1, 2017. Standard Test Methods for Liquid Limit, Plastic Limit, and Plasticity Index of Soils. ASTM International, West Conshohocken, PA.

Atterberg, A., 1911. Über die physikalische Bodenuntersuchung und über die Plastizität der Tone. Int. Mitteilungen für Bodenkunde 10–43.

Babaeian, E., Homaee, M., Montzka, C., Vereecken, H., Norouzi, A.A., 2015. Towards retrieving soil hydraulic properties by hyperspectral remote sensing. Vadose Zone J. 14.

Ben-Dor, E., Banin, A., 1995. Near-infrared analysis as a rapid method to simultaneusly evaluate several soil properties. Soil Sci. Soc. Am. J. 59, 364–372.

Bishop, J.L., Pieters, C.M., Edwards, J.O., 1994. Infrared spectroscopic analyses on the nature of water in montmorillonite. Adv. Agron. 42, 702–716.

Bobrowski, L., Griekspoor, D., 1992. Determination of the plastic limit of a soil by means of a rolling device. Geotech. Test. 15, 284–287.

Brunet, D., Barthès, B.G., Chotte, J.-L., Feller, C., 2007. Determination of carbon and nitrogen contents in Alfisols, Oxisols and Ultisols from Africa and Brazil using NIRS analysis: effects of sample grinding and set heterogeneity. Geoderma 139 (1-2), 106–117.

BS, 2018. Geotechnical Investigation and Testing – Laboratory Testing of Soil. BS EN ISO 17892–12:2018, Part 12: Determination of Liquid and Plastic Limits. International Organisation for Standardization, Switzerland.

Clark, R.N., King, T.V.V., Klejwa, M., Swayze, G.A., Vergo, N., 1990. High spectral resolution reflectance spectroscopy of minerals. J. Geophys. Res.-Solid Earth Planets 95, 12653–12680.

de Jonge, E., Acton, D.F., Stoneohuse, H.B., 1990. Estimating the Atterberg limits of Southern Saskatchewan soils from texture and carbon contents. Can. J. Soil Sci. 70, 543–554.

Fang, Q., Hong, H.L., Zhao, L.L., Kukolich, S., Yin, K., Wang, C.W. 2018. Visible and near-infrared reflectance spectroscopy for investigating soil mineralogy: a review. J. Spectroscopy, 2018.

Gee, G.W., Or, D., 2002. Particle size Analysis. Part 4: Physical Methods. In: Dane, J.H., Topp, G.C. (Eds.), Methods of Soil Analysis. Soils Science Society of America, Madison, pp. 255–293.

Goldshleger, N., Chudnovsky, A., Ben-Dor, E., 2012. Using reflectance spectroscopy and artificial neural network to assess water infiltration rate into the soil profile. Appl. Environ. Soil Sci. 2012, 1–9.

Gupta, A., Das, B.S., Kumar, A., Chakraborty, P., Mohanty, B., 2016. Rapid and noninvasive assessment of atterberg limits using diffuse reflectance spectroscopy. Soil Sci. Soc. Am. J. 80, 1283–1295.

Haigh, S.K., 2012. Mechanics of the Casagrande liquid limit test. Can. Geotech. J. 49, 1015–1023.

Hastie, T., Tibshirani, R., Friedman, J., 2009. The Elements of Statistical Learning: Data Mining, Inference and Prediction. Springer, New York.

Hermansen, C., Knadel, M., Moldrup, P., Greve, M.H., Gislum, R., de Jonge, L.W., 2016. Visible-near-infrared spectroscopy can predict the clay/organic carbon and mineral fines/organic carbon ratios. Soil Sci. Soc. Am. J. 80, 1486–1495.

Hermansen, C., Knadel, M., Moldrup, P., Greve, M.H., Karup, D., de Jonge, L.W., 2017. Complete soil texture is accurately predicted by visible near-infrared spectroscopy. Soil Sci. Soc. Am. J. 81, 758–769.

Houlsby, G.T., 1982. Theoretical-analysis of the fall cone test. Geotechnique 32, 111–118.

Hunt, G., 1977. Spectral signatures of particulate minerals in the visible and near infrared. Geophysics 42, 501–513.

Katuwal, S., Hermansen, C., Knadel, M., Moldrup, P., Greve, M.H., de Jonge, L.W., 2018a. Combining X-ray computed tomography and visible near-infrared spectroscopy for prediction of soil structural properties. Vadose Zone J. 17.

Katuwal, S., Knadel, M., Moldrup, P., Norgaard, T., Greve, M.H., de Jonge, L.W., 2018b. Visible-near-infrared spectroscopy can predict mass transport of dissolved chemicals through intact soil. Sci. Rep. 8.

Kayabali, K., Akturk, O., Fener, M., Ozkeser, A., Ustun, A.B., Dikmen, O., Harputlugil, F., Asadi, R., 2016. Determination of Atterberg limits using newly devised mud press machine. J. Afr. Earth Sci. 116, 127–133.

Keller, T., Dexter, A.R., 2012. Plastic limits of agricultural soils as functions of soil texture and organic matter content. Soil Ressour. 50, 7–17.

Kennard, R.W., Stone, L.A., 1969. Computer aided design of experiments. Technometrics 11 (1), 137–148.

Knadel, M., Arthur, E., Weber, P., Moldrup, P., Greve, M.H., Chrysodonta, Z.P., de Jonge, L.W., 2018. Soil specific surface area determination by visible near-infrared spectroscopy. Soil Sci. Soc. Am. J. 82, 1046–1056.

Knadel, M., de Jonge, L.W., Tuller, M., Rehman, H.U., Jensen, P.W., Moldrup, P., Greve, M.H., Arthur, E., 2020. Combining visible near-infrared spectroscopy and water vapor sorption for soil specific surface area estimation. Vadose Zone 19.

Martens, H., Næs, T., 1989. Multivariate Calibration. John Wiley & Sons, New York.

Mousavi, F., Abdi, E., Ghalandarzadeh, A., Bahrami, H.A., Majnounian, B., Ziadi, N., 2020. Diffuse reflectance spectroscopy for rapid estimation of soil Atterberg limits. Geoderma 361.

Obour, P.B., Jensen, J.L., Lamande, M., Watts, C.W., Munkholm, L.J., 2018. Soil organic matter widens the range of water contents for tillage. Soil Tillage Res. 182, 57–65.

Pasquini, C., 2003. Near infrared spectroscopy: fundamentals, practical aspects and analytical applications. J. Braz. Chem. Soc. 14, 198–219.

Pittaki-Chrysodonta, Z., Arthur, E., Moldrup, P., Knadel, M., Norgaard, T., Iversen, B.V., Jonge, L.W., 2019. Comparing visible-near-infrared spectroscopy and a pedotransfer function for predicting the dry region of the soil-water retention curve. Vadose Zone J. 18 (1), 1–13.

Pittaki-Chrysodonta, Z., Moldrup, P., Knadel, M., Iversen, B.V., Hermansen, C., Greve, M. H., de Jonge, L.W., 2018. Predicting the campbell soil water retention function: comparing visible-near-infrared spectroscopy with classical pedotransfer function. Vadose Zone J. 17.

Post, J.L., Noble, P.N., 1993. The near-infrared combination band frequencies of dioctahedral smectites, micas, and illites. Clays Clay Minerals 41, 639–644.

Rehman, H.U., Knadel, M., Kayabali, K., Arthur, E., 2019. Estimating Atterberg limits of fine-grained soils by visible-near-infrared spectroscopy. Vadose Zone J. 18.

Rossel, R.A.V., Cattle, S.R., Ortega, A., Fouad, Y., 2009. In situ measurements of soil colour, mineral composition and clay content by vis-NIR spectroscopy. Geoderma 150, 253–266.

Rumelhart, D.E., Hinton, G.E., Williams, R.J. 1986. Learning internal representations by error propagation. In: Parallel distributed processing: explorations in the microstructure of cognition, vol. 1 (eds. David, E.R., James, L.M. & Group, C.P.R.), pp. 318-362. MIT Press.

Saikia, A., Baruah, D., Das, K., Rabha, H.J., Dutta, A., Saharia, A., 2017. Predicting compaction characteristics of fine-grained soils in terms of atterberg limits. Int. J. Geosynth. Ground Eng. 3.

Santra, P., Sahoo, R.N., Das, B.S., Samal, R.N., Pattanaik, A.K., Gupta, V.K., 2009. Estimation of soil hydraulic properties using proximal spectral reflectance in visible, near-infrared, and shortwave-infrared (VIS–NIR–SWIR) region. Geoderma 152 (3-4), 338–349.

Savitzky, A., Golay, M., 1964. Smoothing and differentiation of data by simplified least squares procedures. Anal. Chem. 36, 1627–1639.

Scheinost, A.C., 1998. Use and limitations of second-derivative diffuse reflectance spectroscopy in the visible to near-infrared range to identify and quantify Fe oxide minerals in soils. Clays Clay Miner. 46 (5), 528–536.

Schmitz, R.M., Schroeder, C., Charlier, R., 2004. Chemo-mechanical interactions in clay: a correlation between clay mineralogy and Atterberg limits. Appl. Clay Sci. 26, 351–358.

Seybold, C.A., Elrashidi, M.A., Engel, R.J., 2008. Linear regression models to estimate soil liquid limit and plasticity index from basic soil properties. Soil Sci. 173, 25–34.

Sridharan, A., 2014. Soil clay mineralogy and physico-chemical mechanisms governing the fine grained soil behaviour. Indian Geotechn. J. 44, 371–399.

Sivakumar, V., Glynn, D., Cairns, P., Black, J.A., 2009. A new method of measuring plastic limit of fine materials. Geotechnique 59, 813–823.

Smith, C.W., Hadas, A., Dan, J., Koyumdjisky, H., 1985. Shrinkage and Atterberg limits in relation to other properties of principal soil types in Israel. Geoderma 35, 47–65.

Soriano-Disla, J.M., Janik, L.J., Rossel, R.A.V., Macdonald, L.M., McLaughlin, M.J., 2014. The performance of visible, near-, and mid-infrared reflectance spectroscopy for prediction of soil physical, chemical, and biological properties. Appl. Spectrosc. Rev. 49, 139–186.

Spagnoli, G., 2012. Comparison between Casagrande and drop-cone methods to calculate liquid limit for pure clay. Can. J. Soil Sci. 92, 859–864.

Stanchi, S., Catoni, M., D'Amico, M.E., Falsone, G., Bonifacio, E., 2017. Liquid and plastic limits of clayey, organic C-rich mountain soils: role of organic matter and mineralogy. Catena 151, 238–246.

Stenberg, B., Rossel, R.A.V., Mouazen, A.M., Wetterlind, J. 2010. Visible and near infrared spectroscopy in soil science. In: Advances in Agronomy, pp. 163–215.

Suykens, J.A.K., Vandewalle, J., 1999. Least squares support vector machine classifiers. Neural Process. Lett. 9, 293–300.

Waruru, B.K., Shepherd, K.D., Ndegwa, G.M., Kamoni, P.T., Sila, A.M., 2014. Rapid estimation of soil engineering properties using diffuse reflectance near infrared spectroscopy. Biosyst. Eng. 121, 177–185.

Wold, S., Sjostrom, M., Eriksson, L., 2001. PLS-regression: a basic tool of chemometrics. Chemometr. Intelligent Lab. Syst. 58, 109–130.

Yitagesu, F.A., van der Meer, F., van der Werff, H., Zigterman, W., 2009. Quantifying engineering parameters of expansive soils from their reflectance spectra. Eng. Geol. 105, 151–160.

Yukselen-Aksoy, Y., Kaya, A., 2010. Method dependency of relationships between specific surface area and soil physicochemical properties. Appl. Clay Sci. 50, 182–190.